is arranged to be counterbalanced when the wrist unit is midway in its stroke.

- The wrist unit is now designed to be detachable. It is not however "quick-release" in any sense; it takes several minutes to unscrew it from the main unit. But this still allows new wrist designs and other instruments to be developed for the same system as part of future research projects.
- In order to allow macro-micro control in all 3 directions, a 4 degree of freedom wrist was designed for the Black Falcon. To accomodate this wrist, the overall system has 8 powered degrees of freedom instead of 7.
- The Black Falcon is structurally stiffer with higher actuator capacity than the Silver Falcon.
- The carriage on which the wrist unit is mounted uses a much improved bearing and support structure design. It is structurally stiffer, has lower friction, and has a higher load capacity.
- The range of motion of the main pitch and yaw axes of the base have been increased roughly 15 degrees to ± 60 degrees and ± 80 degrees respectively.
- Grip force of the fingers has been increased to a maximum of 240 N (11.1 lbs). The Silver Falcon fingers did not have sufficient grip force to securely hold needles. While it was sufficient to test the primary concepts, actual surgical work was not be possible. The needle would often roll in the grip of the Silver Falcon, much to the frustration of surgeons using the system. The Black Falcon has no difficulty securely holding needles during suturing.
- Unfortunately, the added cabling involved and larger motors used contributes to increased friction in the system.
- However, by modelling the Maxon RE035-071-034 motors with high resolution Canon TR36 laser encoders (14400 counts/rev), a friction compensation algorithm was developed which reduced brush friction by a factor of roughly 4.

6.2 Black Falcon Design

6.2.1 Overview

The following is an overview of the system, and more details will follow in subsequent sections. The Black Falcon consists of a two main subsystems, a base unit and a wrist unit. However, unlike the Silver Falcon, the base unit contains all of the actuators for the entire system and provides a mechanical interconnect for the wrist unit, which is a passive detachable instrument. The following components are referred to in Figure 6-2, and the kinematic structure including axis and link numbers are defined in the schematic drawing Figure 6-3. Note that the 8 joints are labelled 0-7. The system is grounded through a “U”-shaped base. A spindle, link 0, rotates within this base about axis 0. Motor M0 actuates this axis using a cable drive similar to that in the Silver Falcon. Link 1 rotates about axis 1 within the spindle. Link 1 holds motors M1-M7. Motor M1 drives axis 1 using a cable drive similar to axis 0. Motors M1-M7 are all mounted within link 1. The remote center kinematics are formed by links 1-5. Links 1, 3, and 5 are the main structural members, while links 2 and 4 act in tension and compression. Link 5 holds two bearing rails on which a carriage rides. The carriage holds the wrist unit which comprises a mechanical attachment, an instrument shaft, and an end effector consisting of a wrist and grippers.

6.2.2 Base Unit

6.2.2.1 Remote Center Kinematics

We use a similar double parallelagram linkage to form remote center of rotation, as in the Silver Falcon. However, there are offsets in the links now which allow us to place carriage behind remote center in order to give room for our wrist unit.

6.2.2.2 Range of Motion and Workspace

The Black Falcon can pitch forwards and backwards about axis 1 by ± 60 degrees, as shown in Figures 6-4 and 6-5. It can also yaw about axis 0 by ± 80 degrees. Soft stops made from aluminum covered with soft foam rubber have been designed into these two main base axes as a safety measure.

The Black Falcon has a stroke of 20 cm (8 in) with the current version of the wrist unit, and a total carriage travel of 25.4 cm (10 in). The overall workspace is then a cone with an elliptical cross section, which has been truncated with a spherical bottom and top, see Figure 6-6. The centers of the spheres are at the remote center. The height of the cone is the stroke. The location of the truncating surfaces depends on the length of the instrument. For example, if the instrument is shorter, we can access nearer to the remote center. We cannot effectively use the area near the remote center however, because of course the manipulator is singular there. The current wrist unit uses a 38 cm (15 in) instrument shaft which can operate from 3.8 cm (1.5 in) to

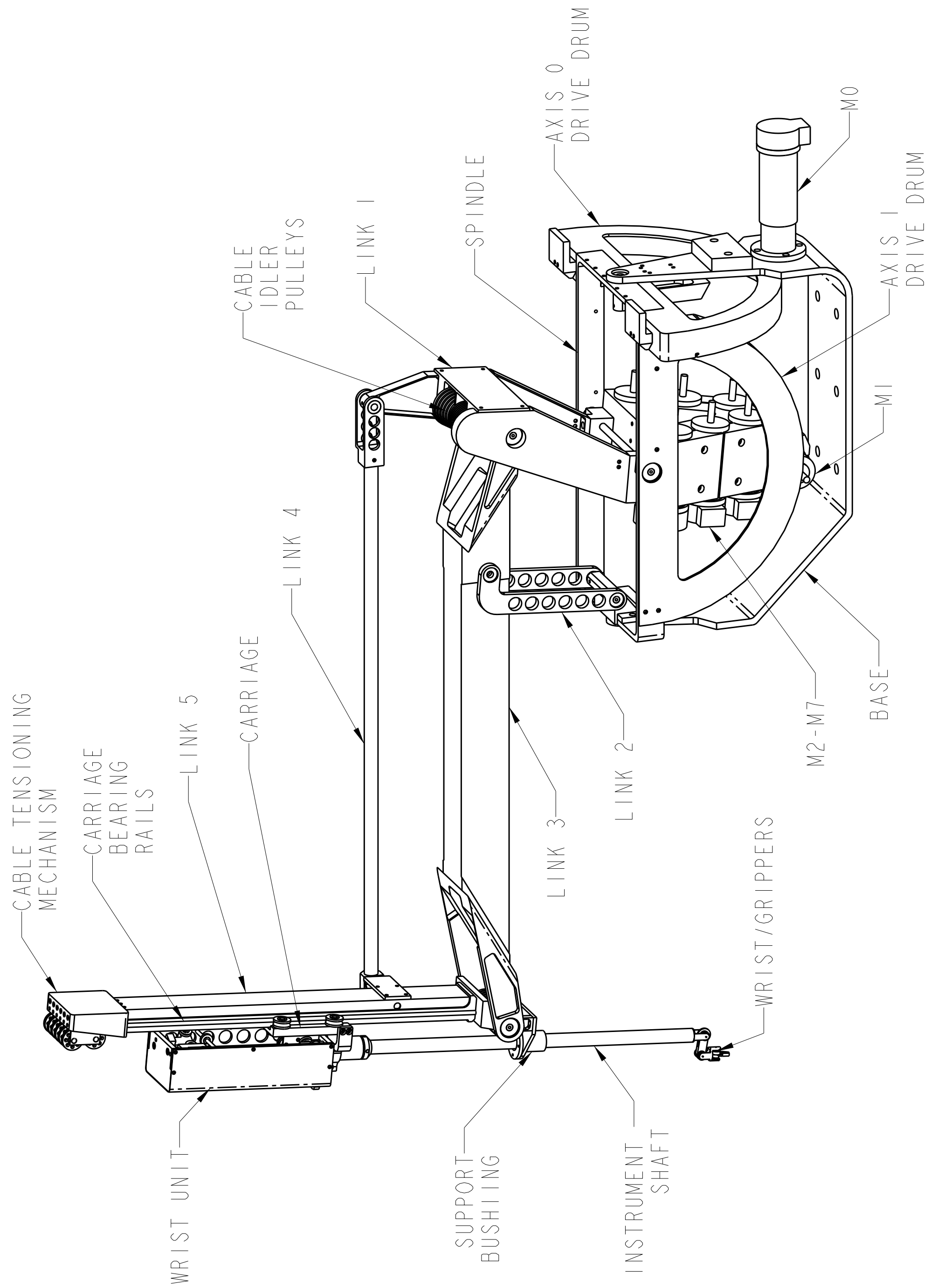

Figure 6-2: The Black Falcon consists of a counterbalanced base unit which carries all the motors for the system. A vertical carriage carries a detachable wrist unit which carries the end effector.

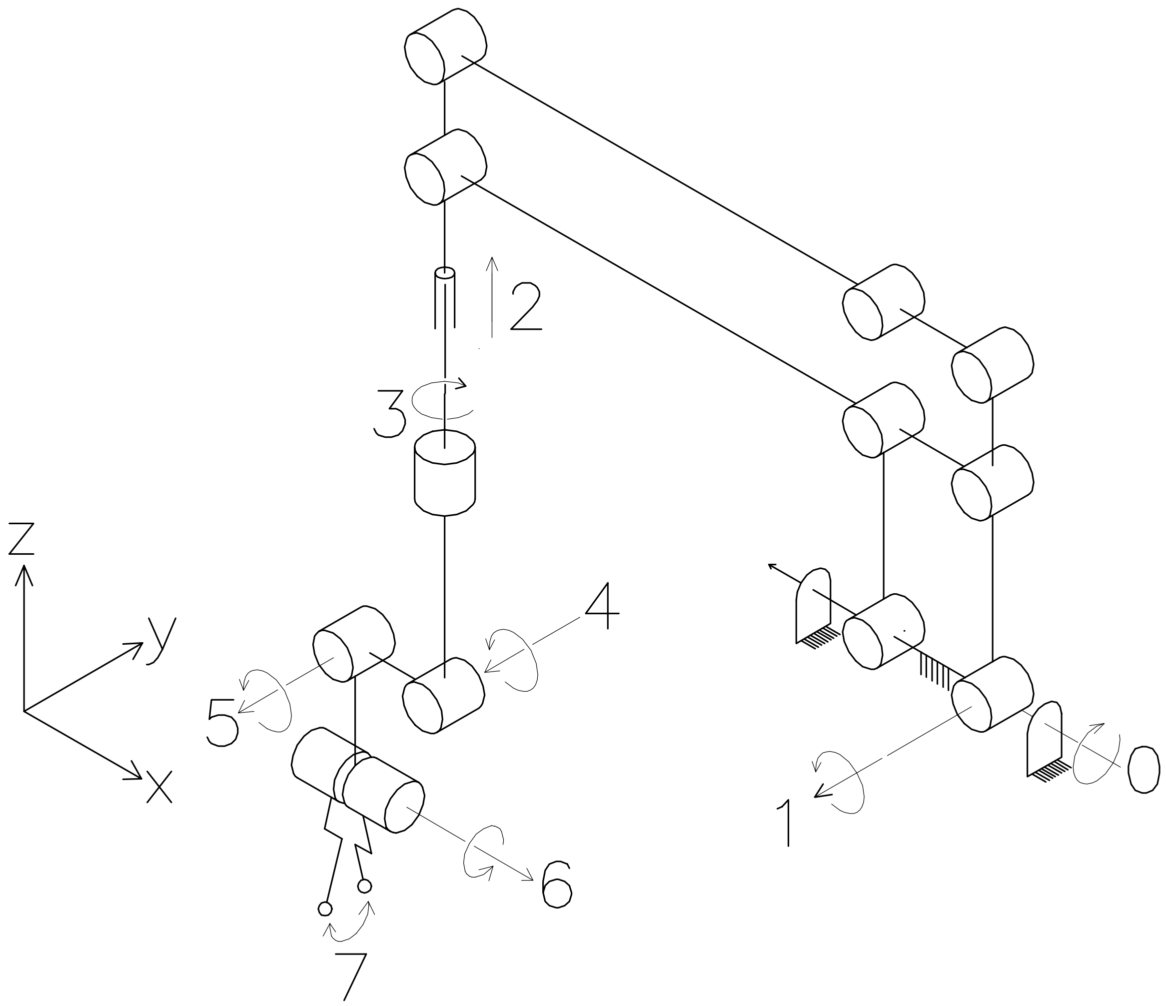

Figure 6-3: The Black Falcon base kinematics are similar to those of the Silver Falcon. However the wrist can now be interchanged, so the system can be redesigned with different wrist kinematics in the future. The wrist we describe has 4 degrees of freedom and is designed to allow macro-micro control in all three linear degrees of freedom. The joint orientations shown are referred to as the "zero" position of the manipulator. Note that we define all joint positions relative their its proximal link *except* joint 5, which is defined relative to ground.

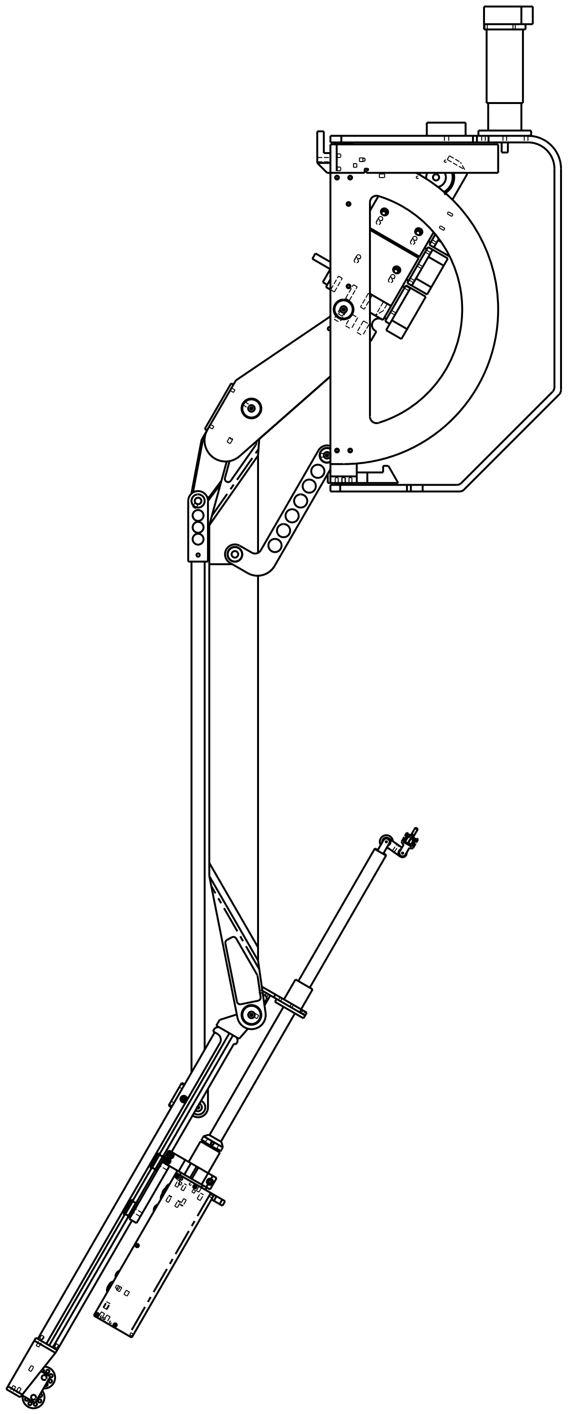

Figure 6-4: The Black Falcon can pitch 60 degrees forwards.

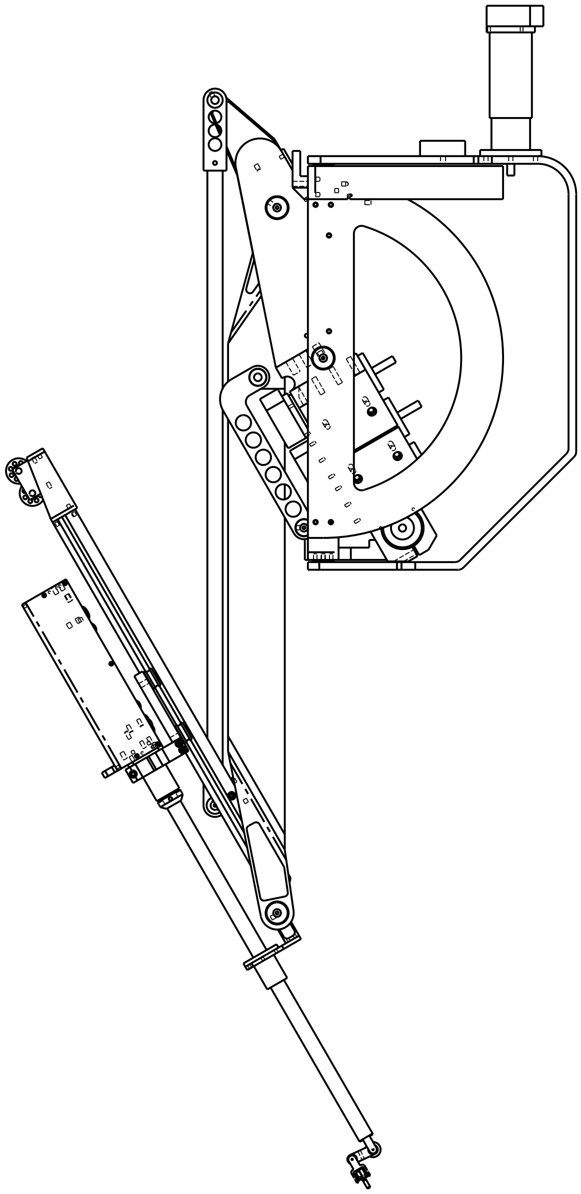

Figure 6-5: The Black Falcon can pitch 60 degrees rearwards. The motors are placed such that they form a "V" which straddles link 3 in order to maximize the rearward pitch angle while still allowing the weight to be placed where it can counterbalance the system.

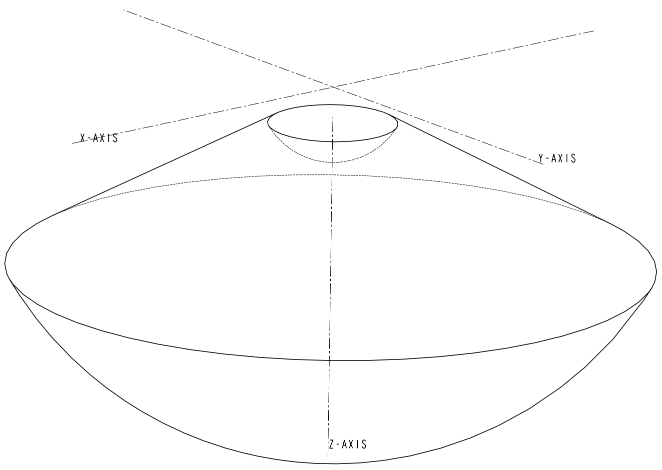

Figure 6-6: The workspace is a elliptical cone truncated with spherical bottom and top surfaces. The axes shown intersect at the remote center.

24 cm (9.5 in) from the remote center.

6.2.2.3 Structure

The structure has been made substantially more rigid. For example, the Silver Falcon link 3 was 1 in diameter aluminum round tubing with 0.035 in wall thickness, whereas the Black Falcon link 3 is 2 in aluminum square box tubing machined to 0.050 in wall thickness. The pivot forks at the end of link 3 have been welded since we found much flexing in the joints of the Silver Falcon. Link 5 is 1 in×1.5 in aluminum square tubing machined to 0.050 in wall thickness.

This beam is 23 in long with pivots connecting it to links 1 and 2 at a distance of 5.5 in apart. To calculate stiffness at the end where link 5 is attached, we assume the link 1 and 2 pivots are simple supports. The deflection δ at this end in response to a force P is given by:

$$\delta = \frac{Pa^2(a+l)}{3EI} \tag{6.1}$$

where in this case $a = 5.5$ in, and $l = 17.5$ in. The tube is 1.85 in×1.85 in (machined down from 2 in square) with a 0.050 wall thickness, so the area moment, I is given by:

$$(1.85^4 - 1.75^4)/12 = 0.0195 \text{ in}^4 \tag{6.2}$$

Given a modulus of elasticity for aluminum, E, of 10.3×10^6 psi, we find:

$$\delta = 0.00117P \text{ in} \tag{6.3}$$
$$k = 3800 \text{ lbs/in} = 150,000 \text{ N/m} \tag{6.4}$$

For example, a 2 lb endpoint force gives a 0.0023 in deflection.

Link 1 consists single aluminum block which houses the 7 motors M1-M7, with 2 aluminum uprights bolted to it. The cable idler pulleys noted in Figure 6-2 are mounted to a piece which braces the two uprights across their backs to add structural stiffness.

We measured stiffness of the base structure by measuring the force (Wagner Force Dial, model FDK 160, Mark 10 Model BG2) required to deflect the end of link 3 by 1/8 in with the base held fixed. It was difficult to measure any deflection in the x direction. Because of the small distaces over which forces could be applied, we can expect accuracy of these values to only about 20%.

$$k_{BY} \cong 5500 \text{ N/m} \tag{6.5}$$
$$k_{BZ} \cong 12000 \text{ N/m} \tag{6.6}$$

Humans find a stiffness of 25,000 N/m indistinguishable from being infinitely rigid, so this is ideally the number we might hope to achieve for the overall system including structural stiffness and servo stiffness of the slave and master. Practically, we would be happy to achieve a total stiffness on the order of 2000 N/m.

6.2.2.4 Base Actuators

The Black Falcon base axes are powered by motors M0 and M1 which are Maxon brushed d.c. servomotors (RE035-071-034) with 4.8:1 planetary gearheads. The additional cable and drum reduction adds approximately 29× reduction to give a total reduction of 137.92:1 for joint 0 and 137.41:1 for joint 1. (The slight difference is caused by manufacturing tolerance.) We typically measure speed reduction by measuring the output link angles using a digital level (Macklanburg-Duncan Pro SmartLevel) and comparing these with encoder readings for five or so points within the range of motion and taking a least squares fit of the results.

One problem with the Silver Falcon was the servo response of the base axes was underdamped due to a lack of encoder resolution and insufficient speed reduction. However, the Black Falcon was designed such that the base actuator rotor inertias were roughly matched to the output load inertia. That is:

$$R \cong \sqrt{\frac{I_{axis0}}{I_{rotor}}}$$

Of course, the inertia about axis 0 varies as axis 1 is moved through its workspace, so it is impossible to match these inertias in all configurations. Using a ProE model of the system, we found the inertia of the system about joint 0 when link 5 is vertical, not including motor inertia, to be 0.183 kgm^2.[1] When the system is pitched rearward by 60° , the inertia is 0.051 kgm^2. The motor rotor inertia is 6.96×10^{-6} kgm^2. Using these two values, we find the reductions required to match the link and rotor inertias at these two configurations to be:

$$R_1 = \sqrt{\frac{0.183}{6.96\times10^{-6}}} = 162 \tag{6.7}$$

$$R_1 = \sqrt{\frac{0.051}{6.96\times10^{-6}}} = 86 \tag{6.8}$$

$$\tag{6.9}$$

The average of these values is 124. As it turns out, we made the ratio slightly larger, that is 137.

We will give experimentally measured inertias for all axes in Section 6.3.4. But we note here that the total joint 0 inertia (link + rotor) calculated using ProE is equal to 0.315 kgm^2 when link 5 is vertical, and the measured joint 0 inertia is 0.32 kgm^2, which gives us confidence in the experimentally measured values and in our CAD system model.

The larger speed reduction also increases effective encoder resolution. On the base axes, we used Hewlett-Packard 5500 series optical encoders with 4096 counts per revolution (after quadrature). With a 137:1 speed reduction, this gives 561,152 counts per joint revolution, or an endpoint resolution of 1.57×10^{-6} m when the instrument shaft is 0.140 m below the remote center, which is the middle of its stroke. Joint step responses are give in Section 6.3.5.

[1]This design was done using ProEngineer CAD software, Parametric Technology Corporation, Waltham MA.

6.2.2.5 Wrist Unit Actuators

Figure 6-7 shows link 1 which houses motors M1-M7. The end effector actuators are all placed within link 1. We use Maxon RE-035-071-034 brushed d.c. motors with Canon TR36 laser encoders. These encoders have 14400 counts per revolution (after quadrature).

Each of the six motors which drive the wrist unit axes is mounted with a threaded drive capstan. The capstan has a flexure clamp manufactured into it to clamp it to the motor shaft. There are flats and screws at each end of the clamp which allow the cable to be terminated on the pinion at each end. The cable is then wound towards the center of the pinion from each end in opposite directions and comes off of the pinion at essentially the same location along the length of the pinion. In this way, slippage on the pinion is impossible, and the extra length required to maintain frictional wraps on the pinion are eliminated. The cable used on these axes is 0.024 in diameter 7×19 cable (Sava Industries, NJ). The motors are placed parallel to one another. This is actually very convenient and allows all the drive cables to emanate from the rear of the link. This works very well with the base cabling scheme which will be described in Section 6.2.2.6.

The motors nearly gravitationally counterbalance the system. To complete and tune the counterbalancing, we placed an additional copper weight of 0.95 kg (2.1 lbs) inside link 1. The weight can be moved forwards and backwards for tuning. The weight incorporates water cooling passages in order to cool the motor block in link 1, see Figure 6-8. Since the motor block is a single piece of aluminum and covers the entire length of the motors, it provides a good heat sink, and can be cooled using the copper counterweight.

The Maxon motors use a rotor which consists of a wire basket set in epoxy. While this gives a low mechanical inertia, it also gives a low thermal inertia making the motors prone to overheating. By water cooling the motors, we can optimally get a factor of 4 improvment in thermal power dissipation. At stall, this corresponds purely to I^2R losses in the rotor and therefore gives a factor of 2 improvement in maximum contintuous torque output. We can see this with a simple calculation based on values from the Maxon Motor catalog. Let:

$$\begin{aligned}
\delta_R &= \text{rotor temperature} \\
\delta_{Rmax} &= \text{max rotor temperature} \\
\delta_U &= \text{ambient temperature} \\
TR_{th} &= \text{total thermal resistance (rotor + ambient)} \\
TR_R &= \text{rotor to housing thermal resistance}
\end{aligned}$$

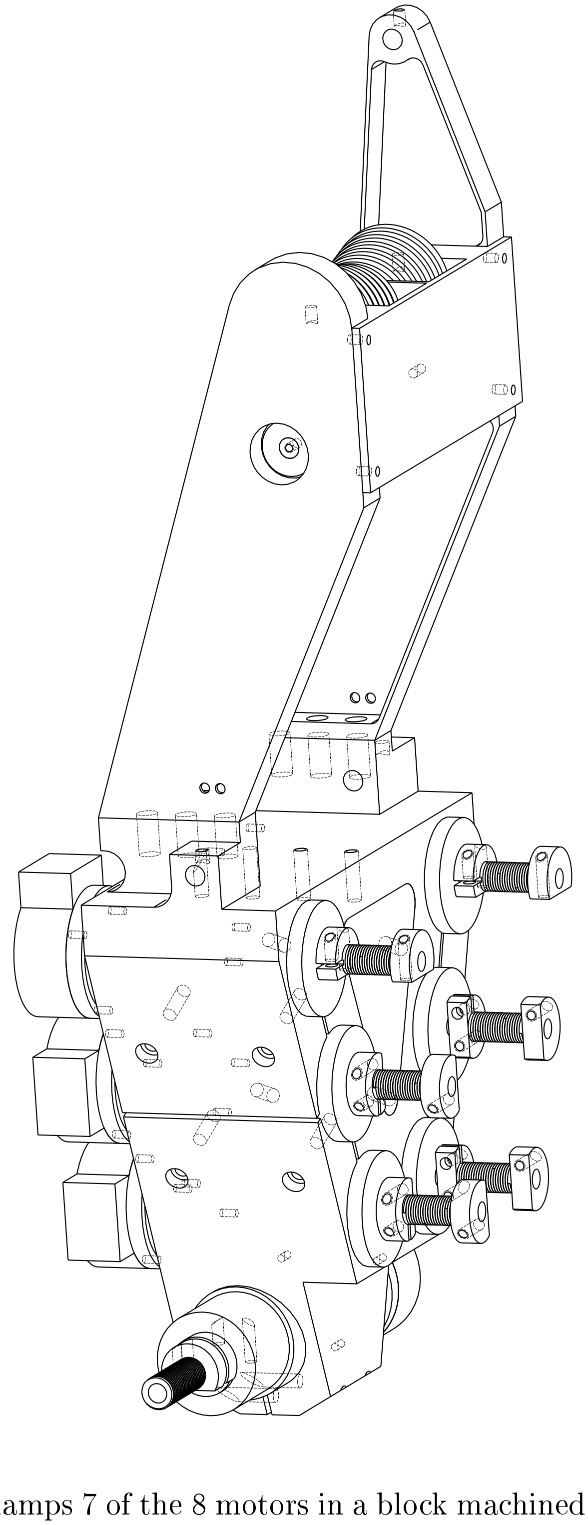

Figure 6-7: Link 1 clamps 7 of the 8 motors in a block machined from a single piece of aluminum. A triangular water-cooled counterweight fits into this piece. Two vertical uprights form and a pulley support piece form the remainder of the structure. Each motor is fitted with a threaded cable drive capstan.

DRAFT

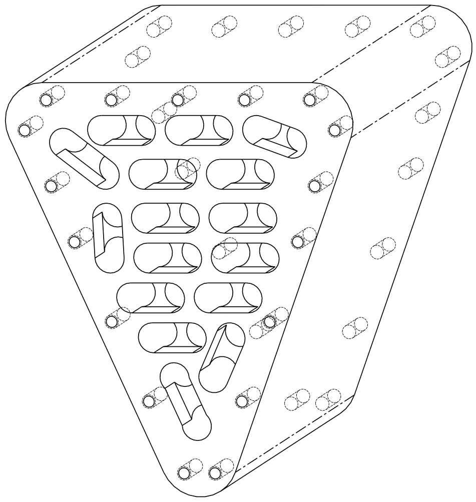

Figure 6-8: The counterweight incorporates radiator like passages for water cooling. It is copper for high thermal conductivity, and use two end plates to form a single continuous water channel.

$$
\begin{aligned}
TR_{ambient} &= \text{housing to ambient thermal resistance} \\
R_R &= \text{rotor electrical resistance} \\
P_J &= \text{power} \\
I_R &= \text{motor rotor current}
\end{aligned}
$$

and using the following values:

$$
\begin{aligned}
\delta_{Rmax} &= 155°\text{C} \\
TR_R &= 2.0°\text{C/W} \\
TR_R &= 6.2°\text{C/W} \\
R_{rotor} &= 2.07\ \Omega
\end{aligned}
$$

We find:

$$P_J = \frac{\delta_R - \delta_U}{TR_{th}} \tag{6.10}$$

$$P_J = \frac{155°\text{C} - 25°\text{C}}{8.2°\text{C}/W} = 15.8\ \text{W} \tag{6.11}$$

The maximum contintuous motor current is then:

$$I_R = \sqrt{P_J/R_R} = 2.77 \text{ A} \tag{6.12}$$

which is slightly higher than the experimentally determined catalog value of 2.15 A. If we maintain the shell of the motor at 25°C, then the thermal resistance is just R_R and we have:

$$P_J = \frac{155°\text{C} - 25°\text{C}}{2.0°\text{C/W}} = 65 \text{ W} \tag{6.13}$$

$$I_R = \sqrt{\frac{65}{2.07\ \Omega}} = 5.6 \text{ A} \tag{6.14}$$

Which represents an approximately $2\times$ increase in continuous torque output.

6.2.2.6 Base Cabling Scheme

We now describe the cabling scheme for each of the 6 motors M2-M7 which lie parallel to each other in link 1. Each of these motors drives a single cable loop. Figure 6-9 shows how this works for one motor. The loop begins by terminating on the motor pinion at point A. The cable continues upwards passing over pulley P1 and under pulley P3. It continues forwards and passes under pulley P5, over pulley P7 and is brought forwards by pulley P8. It then returns around pulleys which lie next to the pulleys it originally passed ppover, pulleys P6, P4, P2 and finally terminating on the motor pinion at point B. Pulleys P3 and P4 lie along a shaft which forms the pivot between links 1 and 3, and pulleys P5 and P6 lie on the shaft which forms the pivot between links 3 and 5. Pulleys P7 and P8 are fixed relative to each other, but can translate along link 5 in order to tension the cable loop. Pulleys P1 and P2 ride on a shaft which is fixed to link 1. Finally, the motor is also fixed to link 1. The nice feature of this cabling scheme is that as the system pitches forwards about axis 1, there is no length change in this cable loop and no coupling between this motion and the motor rotation. [2]

In order to drive the wrist unit, a direct attachment is made between one side of the cable loop between pulleys P5 and P7. We will further describe this below in section 6.2.3.3 after first describing the carriage and wrist unit.

[2]The same method of maintaining constant cable length through a parallelagram motion was used in early mechanical master-slave teleoperators, such as the M8, in the mid 50's, (Vertut and Coiffet, 1986)

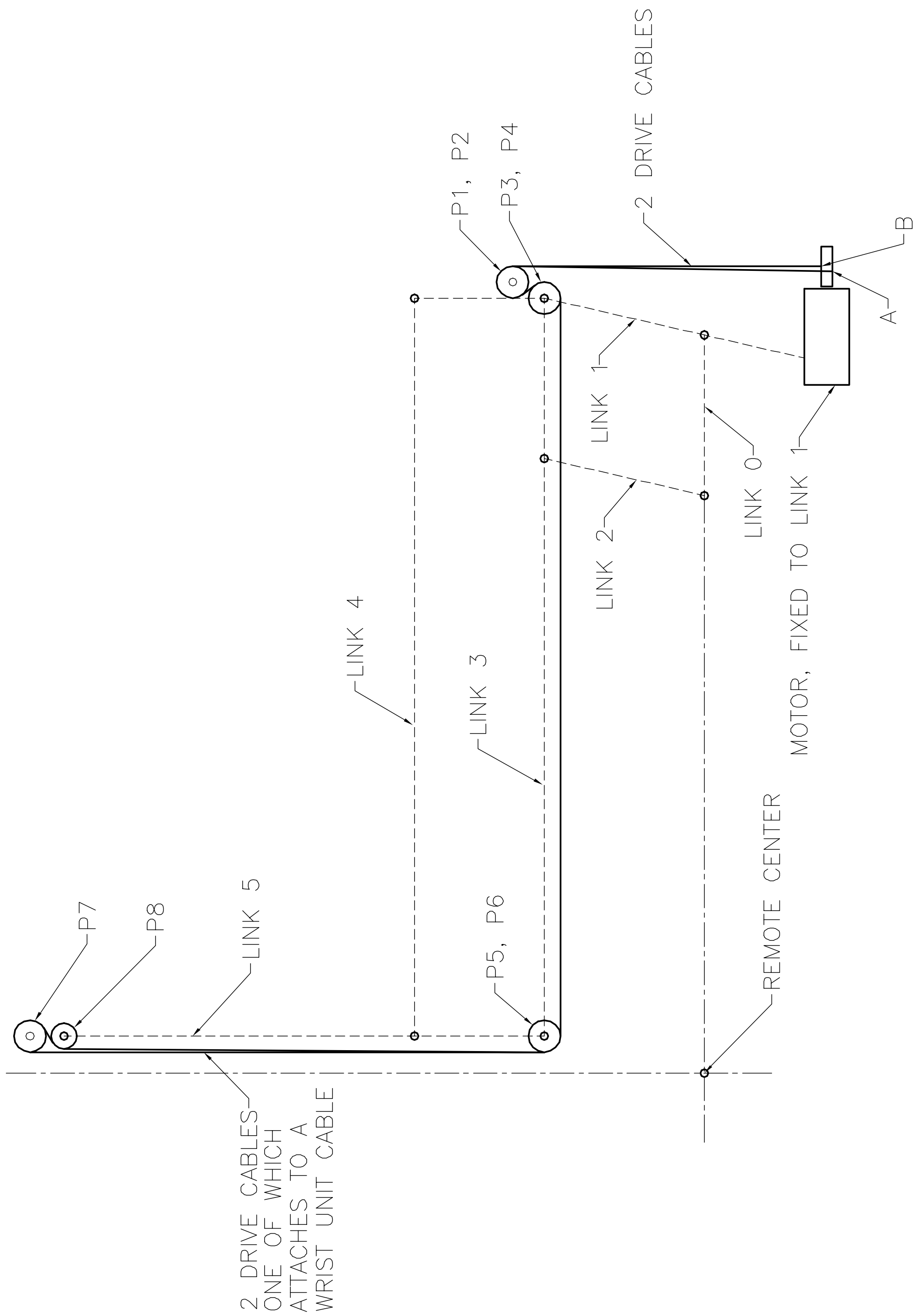

Figure 6-9: The cabling scheme for the base unit allows it to pitch forwards and backwards without moving the cables relative to the carriage. As a result there is no coupling between the base motion and that of the wrist degrees of freedom. The solid line represent mechanical cables, and the dashed lines represent the structure.

6.2.2.7 Carriage

In the Silver Falcon, we designed the bearing system used in the linear axis using Thomson ball bushings riding on 1/4 in diameter steel shafts. This system had several problems. The rigidity of two shafts running parallel to one another is low. Furthermore, the Thompson ball bushings have a dynamic load capacity of only 42 lbs. The Hertzian contact stresses between the balls and the shafts is particularly high in this case because the small balls ride on opposing curvature cylindrical shafts. The friction increases noticably with loading. Finally, the bearings are exposed and are prone to pick up debris or dust on the shafts as they roll by. As a result, they tend to gum up with age.

The new carriage for the Black Falcon uses a different bearing system, see Figure 6-10. Two 4 mm stainless steel rails are mounted in square slots machined into the sides of link 5 to provide bearings ways. The carriage itself uses four INA roller bearings mounted on studs (Part Numbers: LFR 50/5 KDD-4, LFZ 5, LFE 5-0.5) which ride on these steel rails. The bearings themselves are shielded, so that dirt and dust do not interfere with rolling of the balls within them, and lubricant is retained. And the curvature between the INA bearing outer races is designed to match the rails in order to reduce contact stresses. Each of the four bearings has a dynamic load capacity of 269 lbs. The aluminum tubing which comprises link 5 (the carriage beam) is machined from 1×1.5×1/8 in wall aluminum extrusion and is exceedingly stiff in torsion and in bending.

The carriage uses a simple flexure clamp to hold the wrist unit in place. It is designed so that cables run parallel to each other through a space between the clamp carriage. Finally, the carriage beam has a support mounted to the bottom of it to support the slender wrist shaft. The support incorporates a Teflon bushing to reduce friction between the two.

6.2.3 Wrist Unit

The wrist unit is shown in Figure 6-11. It is a seperate assembly which can be detached from the base unit. The cables which drive the wrist form closed pretensioned loops within the wrist unit. The cables are mechanically attached to the base unit cables when the wrist unit is mounted onto the base unit. This attachment is made using simple screw clamps. It is by no means “quick-release”, as it takes several minutes to make the attachment.

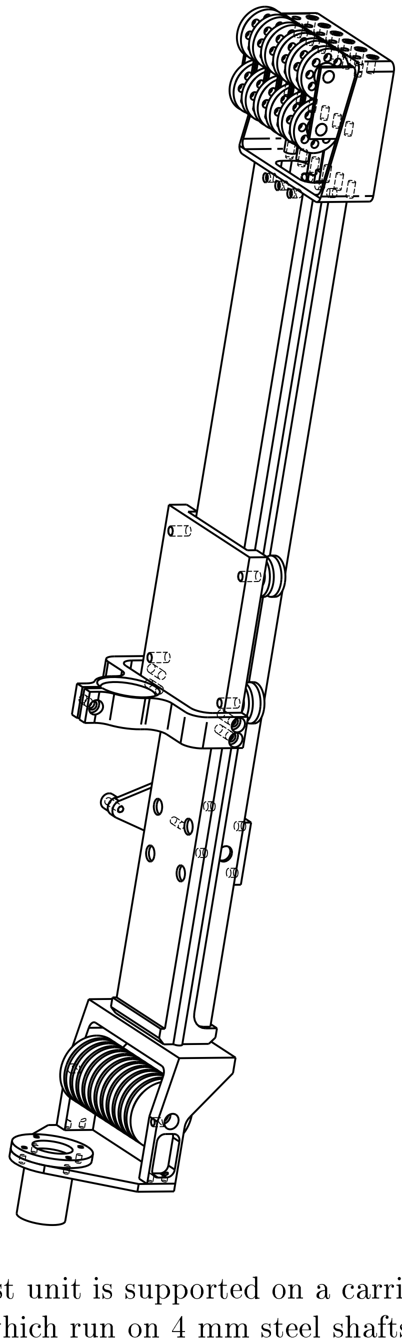

Figure 6-10: The wrist unit is supported on a carriage. This carriage is mounted on INA roller bearings which run on 4 mm steel shafts mounted into grooves machined the carriage beam, which is constructed of machined aluminum box tubing and welded to the lower fork.

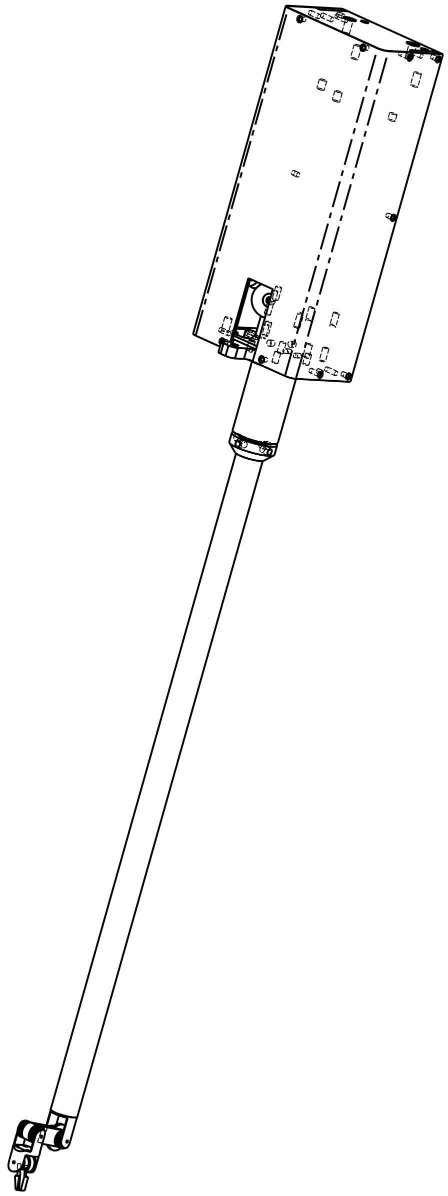

Figure 6-11: The wrist unit is a detachable assembly which clamps to the carriage. The cables directly align with the cables on the main unit and clamp to those cables for attachment.

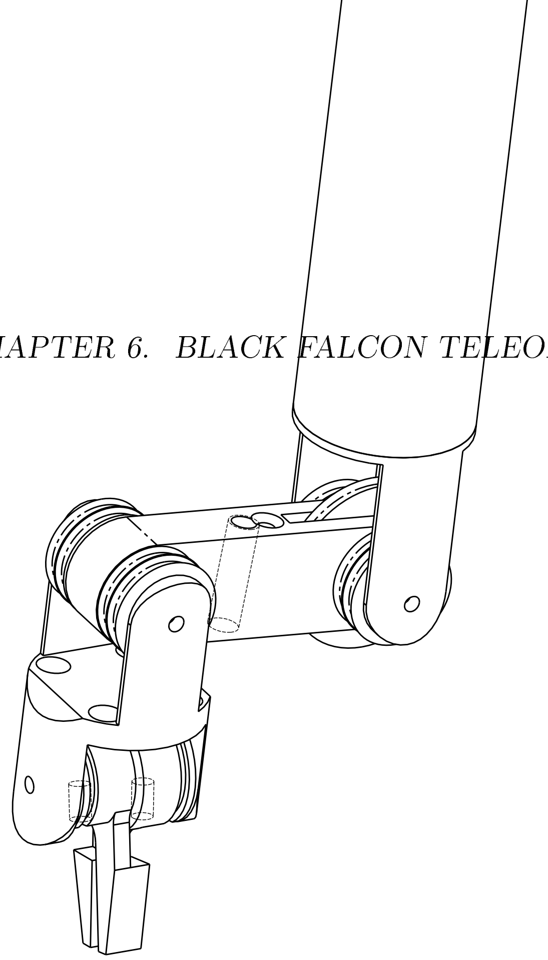

Figure 6-12: This 4 degree of freedom wrist allows macro-micro control in all three directions within ±90° pitch and yaw motions in order to provide force reflection.

6.2.3.1 Wrist Kinematics

Figure 6-12 shows a four degree of freedom wrist developed to improve the use of macro-micro control with the Black Falcon.[3] The wrist is essentially a roll-pitch-pitch-yaw wrist with the first roll being about the instrument shaft. The joint axes are labelled in Figure 6-13, where the gripping freedom is not shown. Recall that to implement macro-micro control, the wrist must allow redundant motions in, ideally, each of three independent directions. The Silver Falcon did this for only two directions. As a result, there was always one direction, pointing directly into the fingers, where redundancy did not exist which resulted in poor force reflection in that direction. The new wrist avoids that problem by adding an extra pitch degree of freedom and maintaining a right-angle bend while reorienting, Figure 6-14. Figure 6-14 shows a number of different orientations which the wrist can assume. By doing so, we maintain a redundant degree of freedom corresponding to motions directly into the fingers.

Unfortunately, such a wrist also has disadvantages. The main disadvantage is that the wrist obviously has a kink in it. There is typically a limited amount of

[3]Note that it is of course possible to use a 3 DOF wrist unit with the Black Falcon if desired, such that the kinematics become the same as those for the Silver Falcon, for example. Since we have already studied these kinematics with the Silver Falcon, we did not reproduce them in a seperate Black Falcon wrist unit.

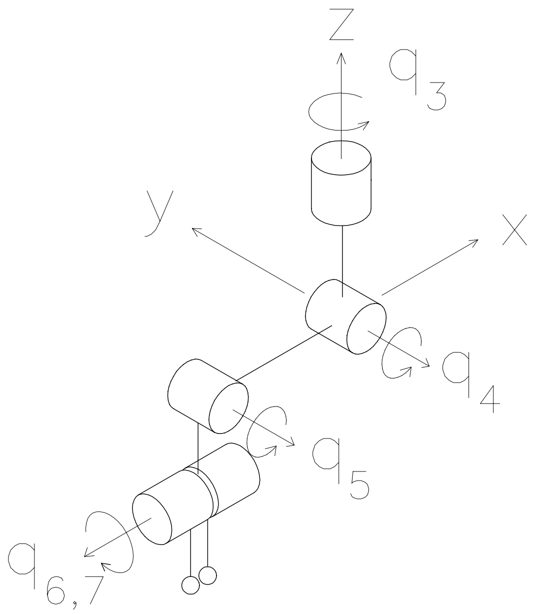

Figure 6-13: Kinematic diagram for the four DOF wrist. We define all joint angles relative to their proximal link emphexcept joint 5 which is defined relative to ground. Therefore in this figure the fingers point horizonatally when $q_5 = \pi/2$ regardless of the position of q_4

.

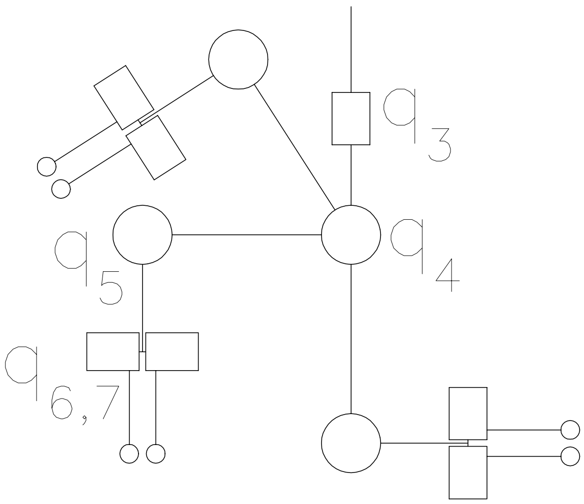

Figure 6-14: The wrist can reorient (pitch) while maintaining a right angle bend in q_6.

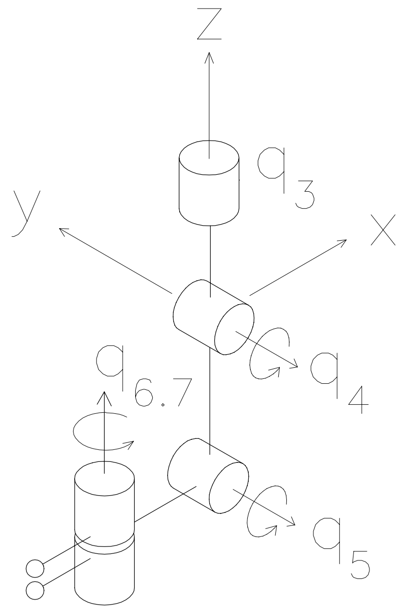

Figure 6-15: The wrist can still be placed in a singular configuration

.

space at the surgical site and the extra room which this wrist occupies may well be a problem. Second, the wrist has essentially the same singularities as does a roll-pitch-yaw wrist. For example, a singlular configuration occurs when the wrist pitch is at $\pi/2$, ($q_5 = \pi/2$) measured from the zero position shown in Figure 6-13, see Figure 6-15.

6.2.3.2 Wrist Cabling and Mechanism

Figure 6-16 shows a schematic diagram of the cabling scheme for the Black Falcon's 4 degree of freedom wrist. The cabling scheme is similar to that for the Silver Falcon with the addition of one joint. The cables for the distal joints simply pass thru this joint on idler pulleys. Two of the six cables which pass thru the instrument shaft actuate joint 4, the joint which has been added. Figure 6-17 shows a schematic of the cable used to drive joint 3, rotation about the instrument shaft.

describe use of alpha wraps describe spectra cable material telfon pulleys, no bearings, rub against each other for side support smaller jaws with knurling for friction.

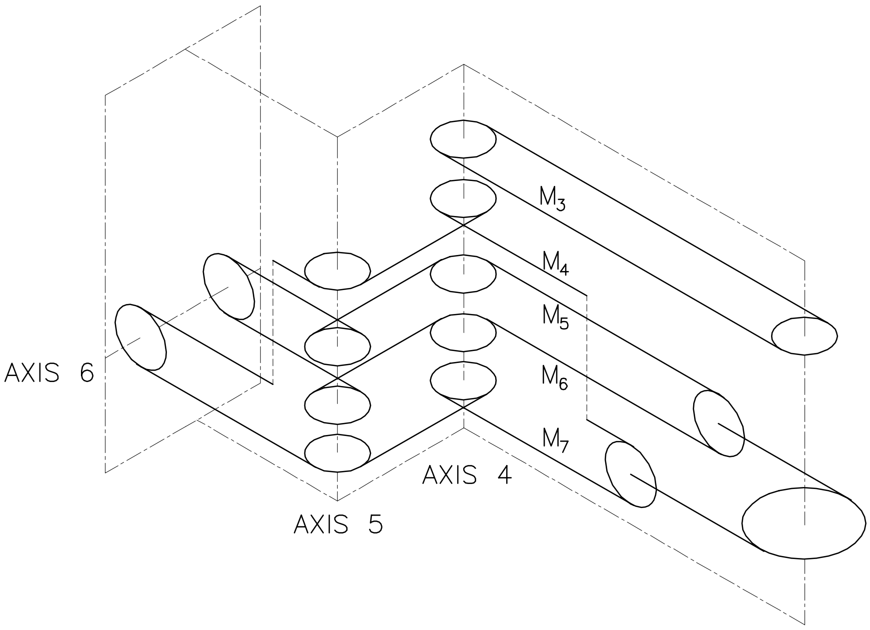

Figure 6-16: The wrist cabling is similar to that of the Silver Falcon, with the addition of one axis. This axis is controlled seperately via an additional cable loop.

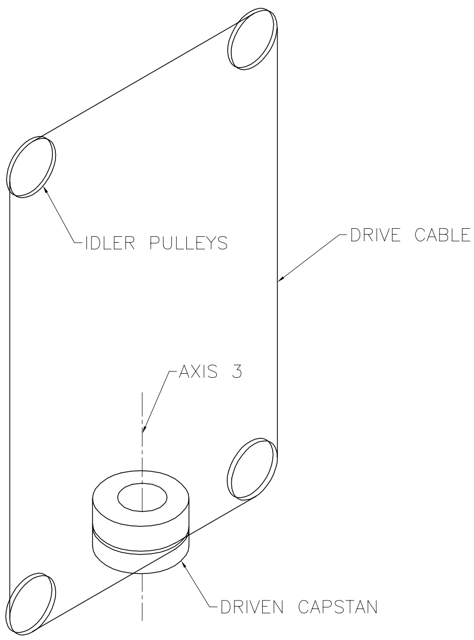

Figure 6-17: Joint 3, rotation about the instrument shaft, is actuated using a cable drive similar to that in the Silver Falcon. One point of the cable loop shown attaches to a drive cable on the base unit.

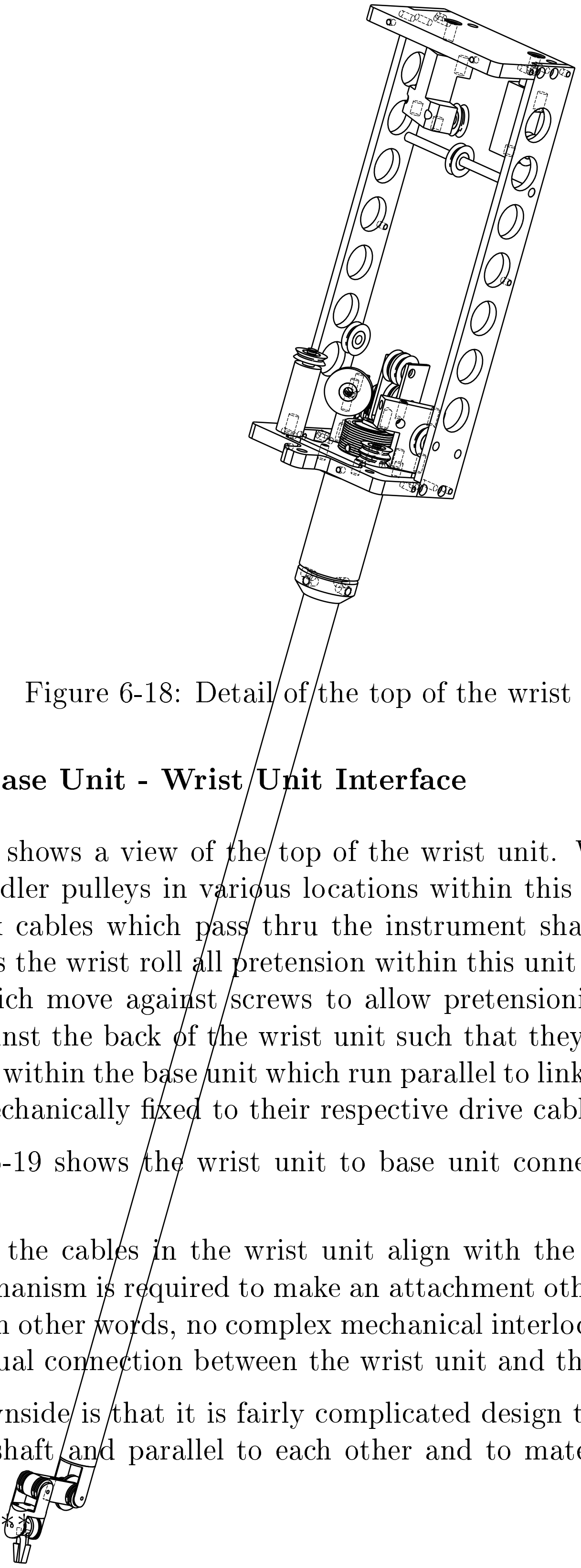

Figure 6-18: Detail of the top of the wrist unit assembly.

6.2.3.3 Base Unit - Wrist Unit Interface

Figure 6-18 shows a view of the top of the wrist unit. What we see is essentially a number of idler pulleys in various locations within this top structure. The effect is that the six cables which pass thru the instrument shaft and the extra cable loop which drives the wrist roll all pretension within this unit against various idler pulleys some of which move against screws to allow pretensioning. Six cable segments are aligned against the back of the wrist unit such that they precisely align with the six drive cables within the base unit which run parallel to link 5. These six cable segments are then mechanically fixed to their respective drive cables using screw clamps.

Figure 6-19 shows the wrist unit to base unit connection for a single degree of freedom.

Because the cables in the wrist unit align with the cables in the base unit, no further mechanism is required to make an attachment other than a single small clamp per cable. In other words, no complex mechanical interlocking mechanism is required, and the actual connection between the wrist unit and the base unit is frictionless.

The downside is that it is fairly complicated design task to get the cables to run out of the shaft and parallel to each other and to mate with the base unit cables.

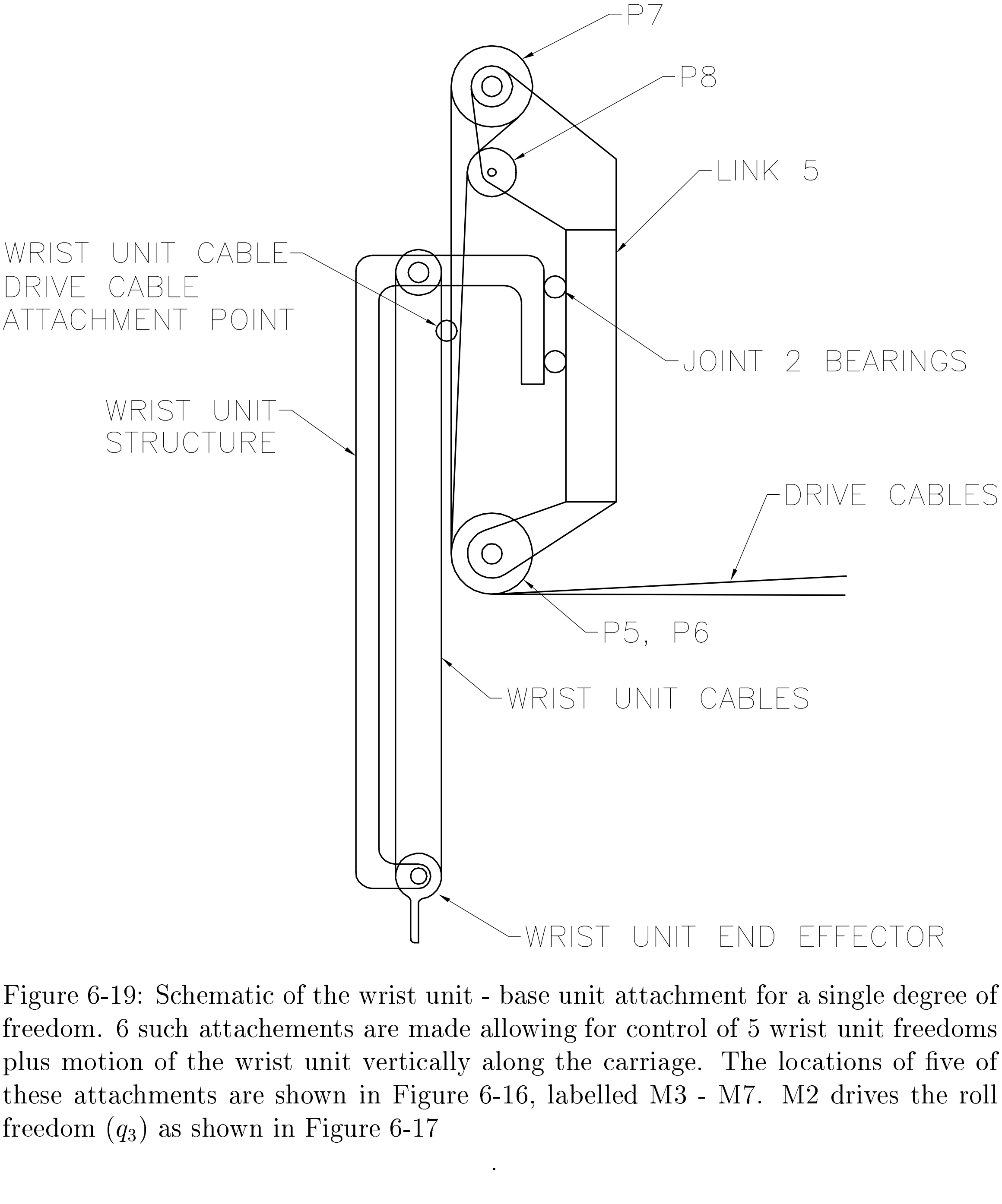

Figure 6-19: Schematic of the wrist unit - base unit attachment for a single degree of freedom. 6 such attachements are made allowing for control of 5 wrist unit freedoms plus motion of the wrist unit vertically along the carriage. The locations of five of these attachments are shown in Figure 6-16, labelled M3 - M7. M2 drives the roll freedom (q_3) as shown in Figure 6-17

.

Also, there is no "quick-release" capability.

6.2.3.4 Differential Kinematics

Here we give the relationships between the motor velocities and joint velocities for joints 2-7. The motor-joint mapping for joints 0 and 1 are simply speed ratios. Let $\mathbf{q}$ be the velocities of joints 2-7, let $\mathbf{c}$ be the velocities of the six drive cables which run parallel to link 5, and let R_3, R_4, R_5, and R_6 be speed ratios defined below:

$$\begin{aligned} R_3 &= 8.717 \times 10^{-3} \text{ m/rad} \\ R_4 &= 6.252 \times 10^{-3} \text{ m/rad} \\ R_5 &= 3.787 \times 10^{-3} \text{ m/rad} \\ R_6 &= 3.094 \times 10^{-3} \text{ m/rad} \end{aligned}$$

We then have:

$$\mathbf{q} = J\mathbf{c} \tag{6.15}$$

where:

$$J = \begin{pmatrix} 1 & 0 & 0 & 0 & 0 & 0 \\ 0 & \frac{1}{R_3} & 0 & 0 & 0 & 0 \\ 0 & 0 & \frac{1}{R_4} & 0 & 0 & 0 \\ 0 & 0 & 0 & \frac{1}{R_5} & 0 & 0 \\ 0 & 0 & 0 & 0 & \frac{1}{R_6} & 0 \\ 0 & 0 & 0 & 0 & 0 & \frac{2}{R_6} \end{pmatrix} \begin{pmatrix} 0 & 1/4 & 1/4 & 1/4 & 1/4 & 0 \\ 0 & 1/4 & 1/4 & 1/4 & 1/4 & -1 \\ -1 & 1/4 & 1/4 & 1/4 & 1/4 & 0 \\ 0 & -1/4 & 1/4 & 1/4 & -1/4 & 0 \\ 0 & -1/4 & -1/4 & 1/4 & 1/4 & 0 \\ 0 & -1/4 & 1/4 & -1/4 & 1/4 & 0 \end{pmatrix} \tag{6.16}$$

6.3 Basic System Performance

We now investigate the performance of the Black Falcon Teleoperator Slave. In this section, we give basic data on a joint by joint basis. The following sections quantify force reflection performance and finally demonstrate suturing.

6.3.1 Joint Limits

The range of motion of each of the joints is given relative to the zero position defined in Figure 6-3.

q_0	$\pm 80°$
q_1	$\pm 60°$
q_2	8 in stroke
q_3	$\pm 180°$
q_4	$-27° \quad +40°$
q_5	$-180° \quad -q_4 \; +30° \quad -q_4$
q_6	$\pm 100°$
q_7	$+200°$ jaw opening

6.3.2 Structural Stiffness

The structural stiffness at the endpoint of the system is given below. These numbers are difficult to measure and are probably accurate to about 20%. We calculated stiffness by measuring the force required to deflect the instrument shaft by 1/16 in in the x direction and 1/8 in in the y direction using a force gage (Mark 10 Model BG2). The z direction structural stiffness is that found for the base unit in section 6.2.2.3, and is repeated below:

$$\begin{aligned} k_{WX} &\cong 9500\ N/m \\ k_{WY} &\cong 2800\ N/m \\ k_{WZ} &\cong 12000\ N/m \end{aligned}$$

These measurements were made with the wrist unit centered in its stroke. The point where force was applied was .15 m (6 in) below the teflon support bushing, and 0.086 m (3.4 in) below the remote center.

6.3.3 Friction

We measured the force required to backdrive each joint of the wrist with the base joints 0 and 1 held stationary, and when the manipulator was in its zero postion (Figure 6-13). We made 4 - 6 measurements in each case and averaged the results. The forces we measured were:

- f_R is a force in x direction applied in line with axis 5, which causes rotation about axis 3 only.
- f_X is a force at the finger tips in the x direction with the fingers closed. Axis 3 is held fixed, so only axis 6 may rotate.
- f_Y is a force at the finger tips in the y direction. Only axis 5 rotates.
- f_Z is a force at tip in z direction. Only axis 4 rotates.
- f_{q2} is the force required to backdrive the carriage and wrist unit together.

In the first case, we measured these forces with the system turned completely off.

$$\begin{aligned} f_R &= 0.63 \pm 0.04 \text{ N} \\ f_X &= 1.1 \pm 0.2 \text{ N} \\ f_Y &= 0.60 \pm 0.2 \text{ N} \\ f_Z &= 0.96 \pm 0.06 \text{ N} \\ f_{q2} &= 12.9 \pm 0.03 \text{ N} \end{aligned}$$

In the second case, we turned our friction compensation algorithm on and measured the same forces.

describe friction comp algorithm.

$$\begin{aligned} f_R &= 0.48 \pm 0.1 \text{ N} \\ f_X &= 0.88 \pm 0.14 \text{ N} \\ f_Y &= 0.40 \pm 0.02 \text{ N} \\ f_Z &= 0.73 \pm 0.07 \text{ N} \\ f_{q2} &= 2.86 \pm 0.2 \text{ N} \end{aligned}$$

The friction is created in two places, within the wrist itself and in the motors as brush friction. The fact that joint 2 friction can be reduced by a factor of 4 indicates that this axis is dominated by brush friction because this is what the friction compensation algorithm compensates for. However, in the other cases where the compensation does not reduce overall friction substantially, the friction must be directly in the wrist.

6.3.4 Inertia

The inertias of each joint were calculated by plotting oscillatory step reponses where very little damping and a known spring constant (position gain) were used. These were compared to a simulation of a spring mass damper system. The simulation mass and damping were modified until a fit was found to find the actual mass and damping.

$$
\begin{aligned}
I_0 &= 0.32 \text{ kgm}^2 \\
I_1 &= 0.25 \text{ kgm}^2 \\
I_2 &= 3.35 \text{ kg} \\
I_3 &= 26.0 \times 10^{-6} \text{ kgm}^2 \\
I_4 &= 20.0 \times 10^{-6} \text{ kgm}^2 \\
I_5 &= 20.5 \times 10^{-6} \text{ kgm}^2 \\
I_6 &= 19.5 \times 10^{-6} \text{ kgm}^2 \\
I_7 &= 2.8 \times 10^{-6} \text{ kgm}^2
\end{aligned}
$$

6.3.5 Individual Joint Responses

This section is essentially a compendium of joint responses in order to give a quantitative idea of how well the system performs on a joint by joint basis.

In order to give an idea of the position servo performance available with the Black Falcon, we give individual joint responses for a fairly well tuned set of gains given below:

$$
\begin{array}{ll}
K_{qs0} = 3500 \text{ Nm/rad} & B_{q0} = 35 \text{ Nms/rad} \\
K_{qs1} = 3500 \text{ Nm/rad} & B_{q1} = 35 \text{ Nms/rad} \\
K_{qs2} = 20000 \text{ N/m} & B_{q2} = 200 \text{ Ns/m} \\
K_{qs3} = 1.5 \text{ Nm/rad} & B_{q3} = 0.015 \text{ Nms/rad} \\
K_{qs4} = 0.8 \text{ Nm/rad} & B_{q4} = 0.008 \text{ Nms/rad} \\
K_{qs5} = 0.3 \text{ Nm/rad} & B_{q5} = 0.003 \text{ Nms/rad} \\
K_{qs6} = 0.2 \text{ Nm/rad} & B_{q6} = 0.002 \text{ Nms/rad} \\
K_{qs7} = 0.05 \text{ Nm/rad} & B_{q7} = 0.0005 \text{ Nms/rad}
\end{array}
$$

During master-slave teleoperation we used much lower joint 0 and 1 gains, because the system was no longer stable at these high gains. We suspect this is due to limited position measurement resolution in the Phantom master. Consider that a joint 0 gain of 3500 N/m corresponds to an endpoint stiffness of 128,400 N/m when the tip of the fingers are at a distance of 0.17 m from the remote center. This is an extremely high endpoint stiffness. The endpoint resolution about joint 0 is the result of a 4096 count encoder and a 137:1 speed reduction, which gives 561,152 counts/rev or at 0.17 m a

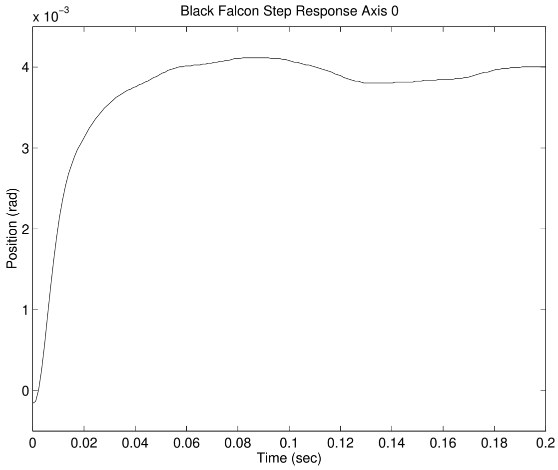

Figure 6-20: Joint 0 response to a 0.004 rad step input.

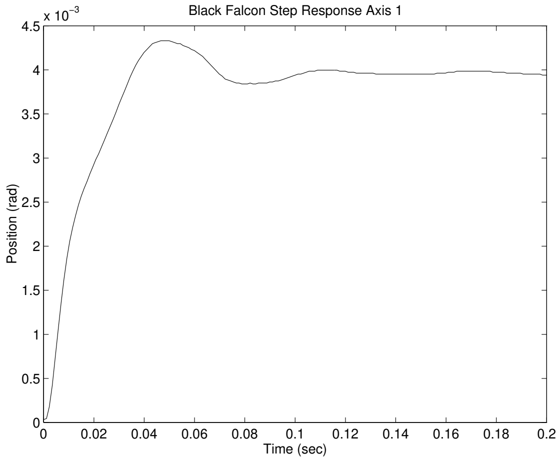

Figure 6-21: Joint 1 response to a 0.004 rad step input.

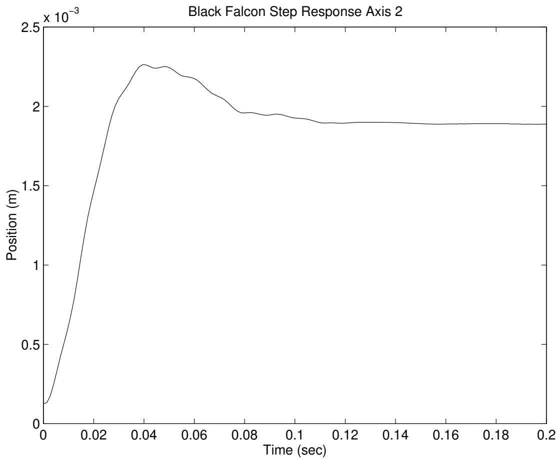

Figure 6-22: Joint 2 response to a 0.002 m step input. Gain used during force reflection tests.

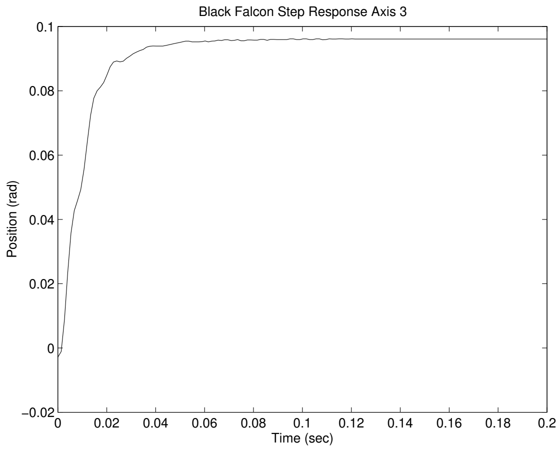

Figure 6-23: Joint 3 response to a 0.1 rad step input.

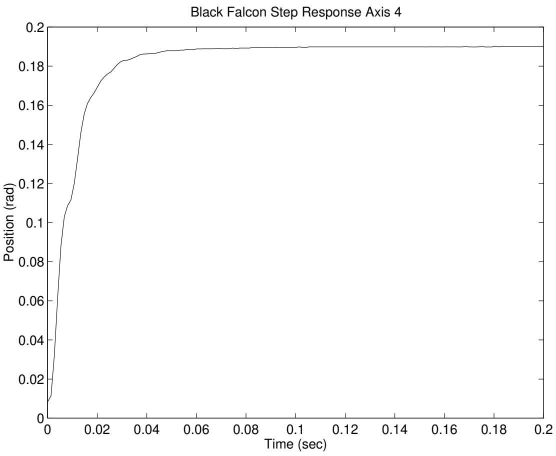

Figure 6-24: Joint 4 response to a 0.2 rad step input.

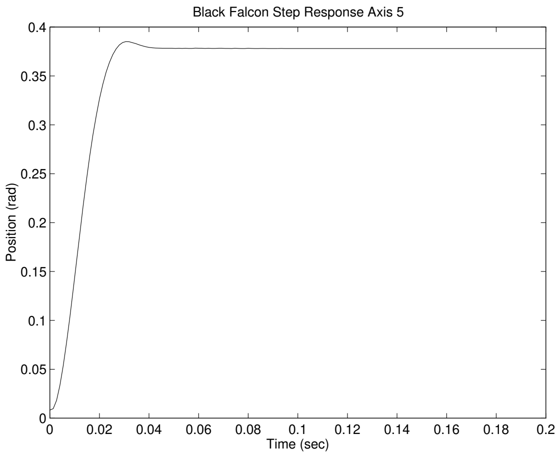

Figure 6-25: Joint 5 response to a 0.4 rad step input.

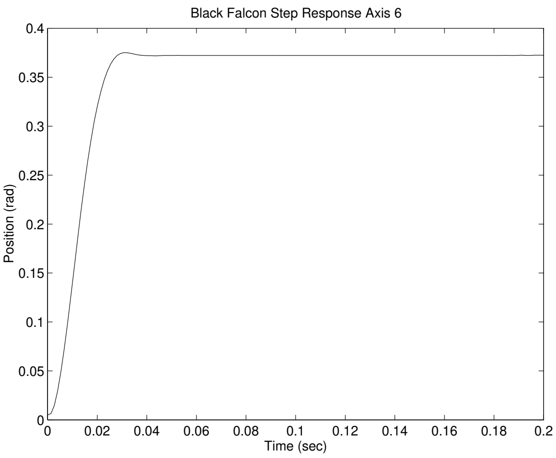

Figure 6-26: Joint 6 response to a 0.4 rad step input.

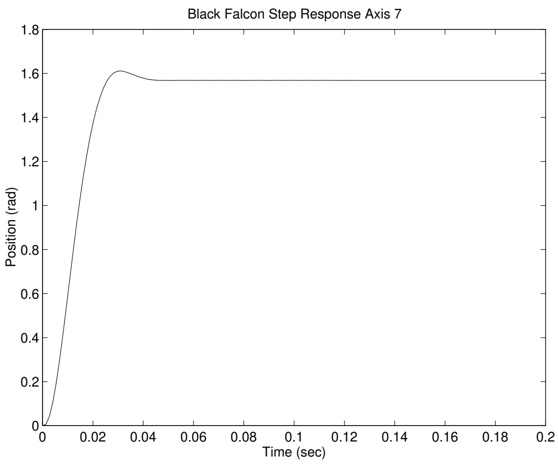

Figure 6-27: Joint 7 response to a 1.6 rad-step input.

3.03×10^{-7} m resolution. The inertia of this axis is high, at 0.32 kgm^2, so that the bandwidth of the response is only $\sqrt{3500/0.32} = 104$ rad/sec $\cong 17$ Hz. With such high positioning resolution and inertia, it is no wonder we can achieve such high stiffness. However, the Phantom has an endpoint resolution of 4.511×10^{-5} m. Therefore, if the slave tracks the master at this high gain, each time the master moves by one encoder tick, the slave sees a force step of 5.8 N or 1.3 lbs. Tracking such a coarse input creates noticable vibration in the system.

Also, the slave has a structural flexibility at roughly 8-12 Hz as we can see in Figures 6-20 and 6-21. We believe the vibration caused by tracking the coarse master input combined with these structural dynamics is causing instability at high gains and has forced us to detune the slave joint 0 and 1 gains to 200 Nm/rad, which corresponds to an equivalent endpoint stiffness of 6900 N/m. One encoder tick movement on the master now corresponds to a 0.31 N (0.07 lb) force step for the slave.

The second reason our gains are different during the force reflection tests is that we need to adjust them appropriately in order to have a 2:1 force scaling. Because we are now running joint P.D. gains (instead of a cartesian P.D. mapped to joints via J^T) we must set the joint gains to give an endpoint gain which is 1/2 that of the master, or 240 N/m. These gains are dependent on the conguration of the wrist. For our force reflection tests, where the manipulator was always nominally in its zero position (Figure 6-3) we used the gains given below:

$$
\begin{array}{ll}
K_{qs0} = 200 \text{ Nm/rad} & B_{q0} = 10 \text{ Nms/rad} \\
K_{qs1} = 200 \text{ Nm/rad} & B_{q1} = 10 \text{ Nms/rad} \\
K_{qs2} = 20000 \text{ N/m} & B_{q2} = 250 \text{ Ns/m} \\
K_{qs3} = 0.12 \text{ Nm/rad} & B_{q3} = 0.004 \text{ Nms/rad} \\
K_{qs4} = 0.10 \text{ Nm/rad} & B_{q4} = 0.003 \text{ Nms/rad} \\
K_{qs5} = 0.20 \text{ Nm/rad} & B_{q5} = 0.004 \text{ Nms/rad} \\
K_{qs6} = 0.10 \text{ Nm/rad} & B_{q6} = 0.003 \text{ Nms/rad} \\
K_{qs7} = 0.04 \text{ Nm/rad} & B_{q7} = 0.0007 \text{ Nms/rad}
\end{array}
$$

6.4 Force Reflection

In this section we discuss force reflection only for the Jacobian Inverse controller, see Chapter 3. We found good force reflection with this controller. When programmed with the Jacobian Transpose controller, it is essentially impossible to move the slave using the master due to its large apparent inertia. We also found some success using the Simulated Force Sensor controller, though we do not present results here.

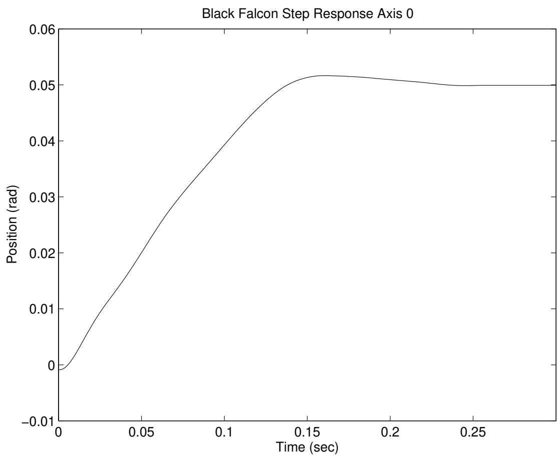

Figure 6-28: Joint 0 response to a 0.004 rad step input. Gains used during force reflection tests.

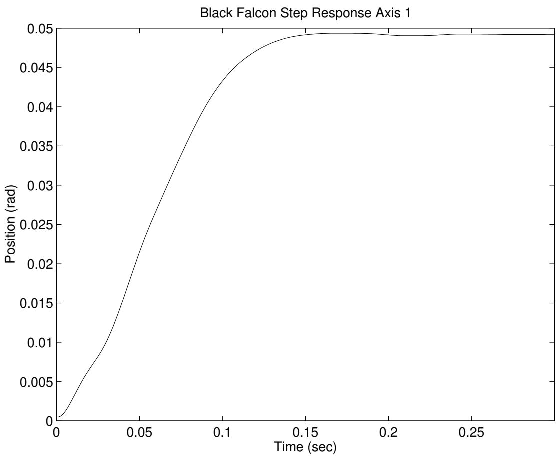

Figure 6-29: Joint 1 response to a 0.004 rad step input. Gains used during force reflection tests.

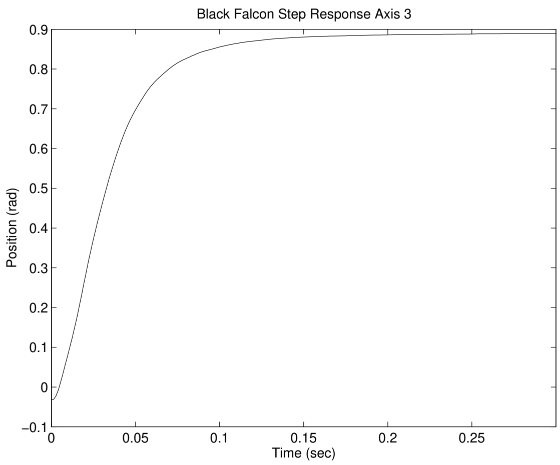

Figure 6-30: Joint 3 response to a 0.1 rad step input. Gains used during force reflection tests.

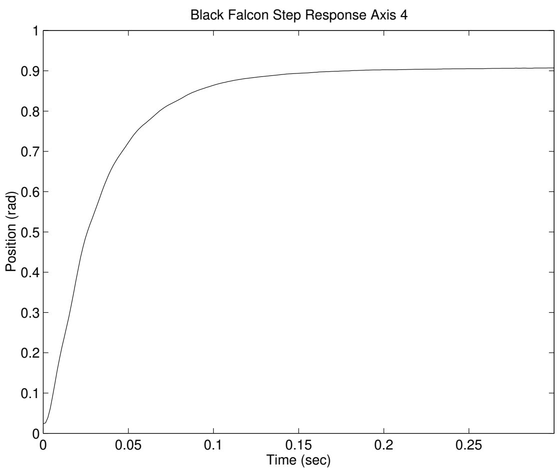

Figure 6-31: Joint 4 response to a 0.2 rad step input. Gains used during force reflection tests.

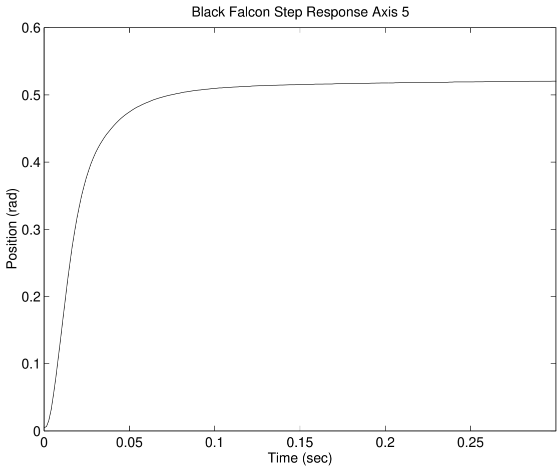

Figure 6-32: Joint 5 response to a 0.4 rad step input. Gains used during force reflection tests.

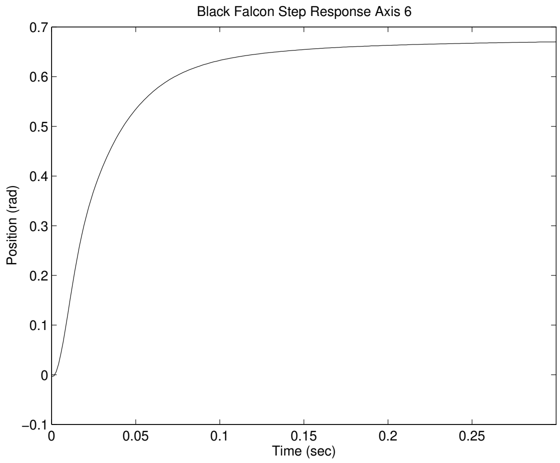

Figure 6-33: Joint 6 response to a 0.4 rad step input. Gains used during force reflection tests.

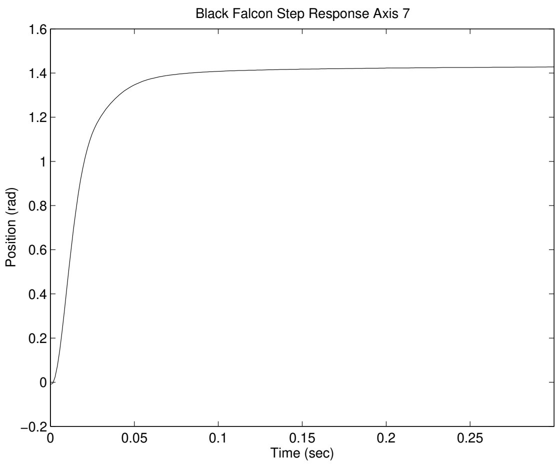

Figure 6-34: Joint 7 response to a 1.6 rad step input. Gains used during force reflection tests.

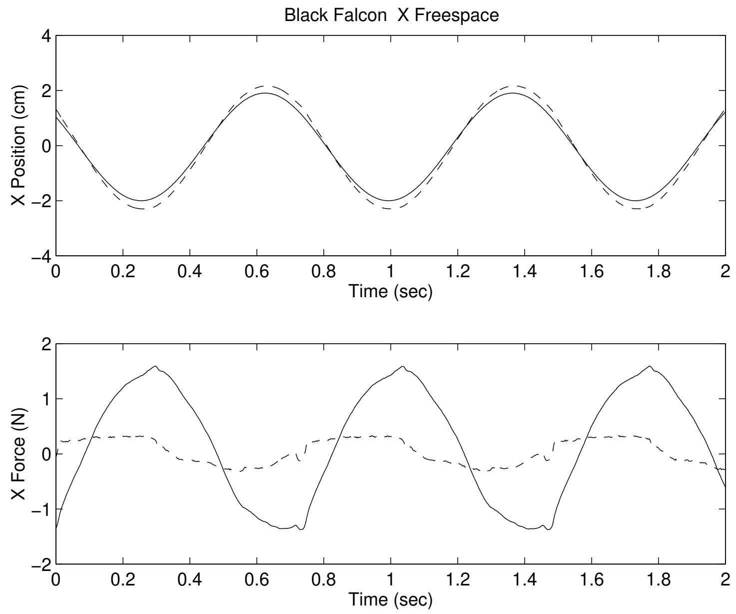

Figure 6-35: Freespace response for the Black Falcon slave and Phantom master in the x direction using the Inverse Jacobian controller. The solid line represents the master, and the dashed line represents the slave.

6.4.1 Freespace Responses

Figures 6-35 and 6-36 show freespace response in the x and y directions, which are quite similar. As in the Silver Falcon, we see a substantial amount of tracking error which is presented as a a force of roughly 1.5 N to the master. Our first reaction is that this error should not exist given that we went through some effort to improve the base tracking ability of the Black Falcon. Recall though that we *lowered* the base gains from a possible 3500 Nm/rad to 200 Nm/rad during these tests. The result is diminished base tracking and hence diminished freespace performance.

The z axis tracking performance is considerably better, Figure 6-37. In absolute terms, the tracking error is less. This case is different from the x and y direction cases in that the error here is due to the micro axis more than the macro axis. The macro axis (joint 2) is in running at a high (20,000 N/m) gain which unlike in the joint 0 and 1 axes does not seem to cause vibration. This is likely because structural stiffness is higher in this direction and the inertia being moved is considerably less.

Joint 4 acts as the micro axis during the z direction tests. It is coupled to joint 2 (through the cable drive) such that when the direction of motion of joint 2 changes, a force equivalent to the joint 2 backdrive friction is introduced to the joint 4 and

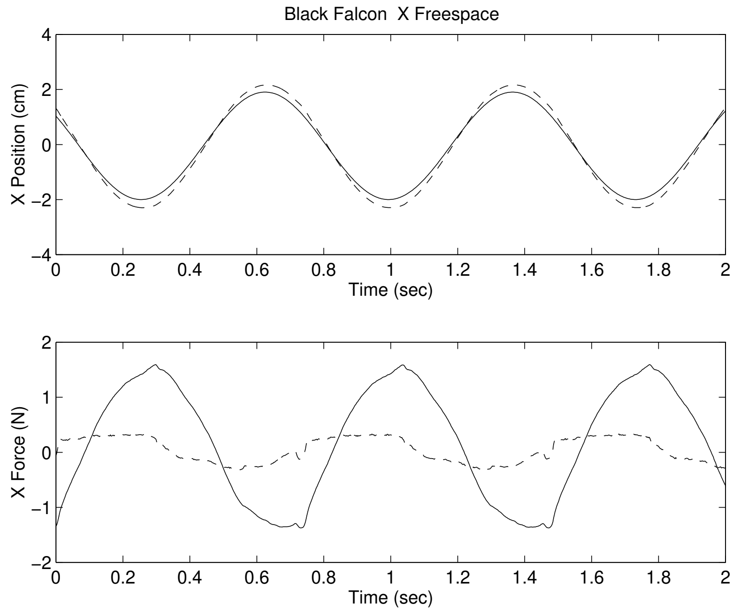

Figure 6-36: Freespace response for the Black Falcon slave and Phantom master in the y direction using the Inverse Jacobian controller. The solid line represents the master, and the dashed line represents the slave.

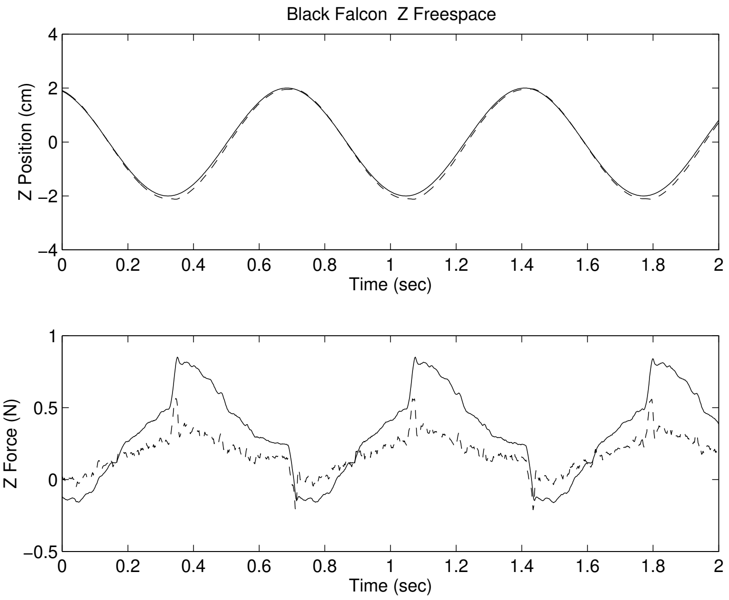

Figure 6-37: Freespace response for the Black Falcon slave and Phantom master in the z direction using the Inverse Jacobian controller. The solid line represents the master, and the dashed line represents the slave.

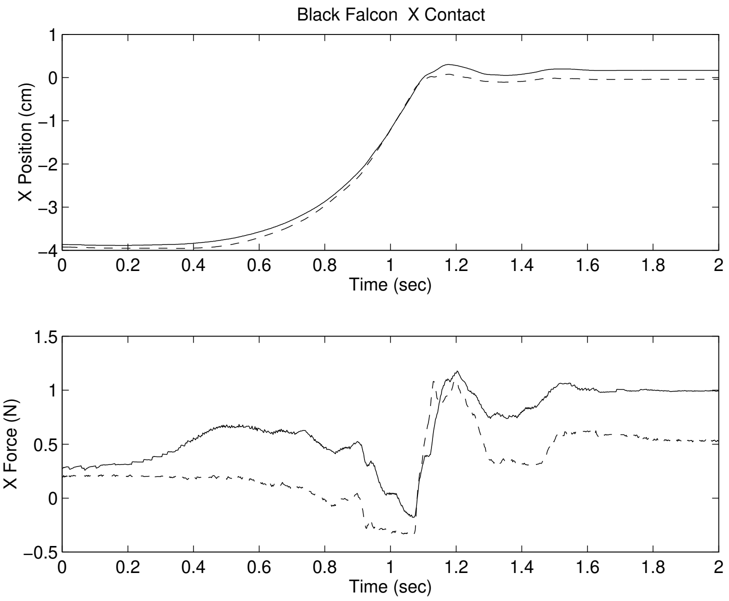

Figure 6-38: Contact response for the Black Falcon slave and Phantom master in the x direction using the Inverse Jacobian controller. The solid line represents the master, and the dashed line represents the slave.

hence the output. This explains the cyclic sharp rise and fall in the output error plot when the direction of motion changes.

6.4.2 Contact Responses

mention that we use the Phantom here.

Again, the x and y direction plots look similar, Figures 6-38 and 6-39. We have as we should expect fairly substantial freespace forces resulting from the low values of the base gains used. The contact is however, quite good. We see sharp force increases in both the master and the slave which closely mimick each other. The steady state forces settles to 0.5 N and 1.0 N showing the 2:1 force scaling implemented.

Also note that there is little overshoot seen in the measured slave tip position as it contacts the aluminum block. This means our estimate of the endpoint postion using joint measurements is good and that there is less structural flexibility than there was in the Silver Falcon.

The z direction contact response is considerably better, Figure 6-40. This is in fact what we had hoped they would all look like. The tracking performance is excellent

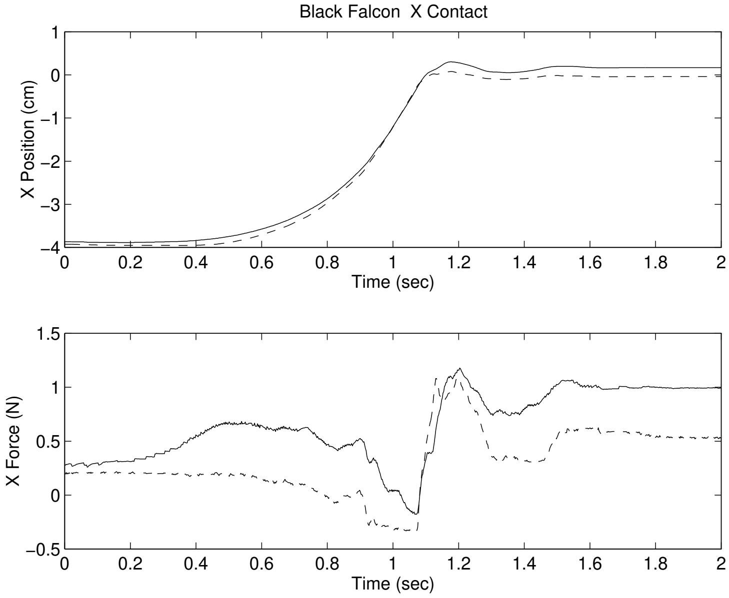

Figure 6-39: Contact response for the Black Falcon slave and Phantom master in the y direction using the Inverse Jacobian controller. The solid line represents the master, and the dashed line represents the slave.

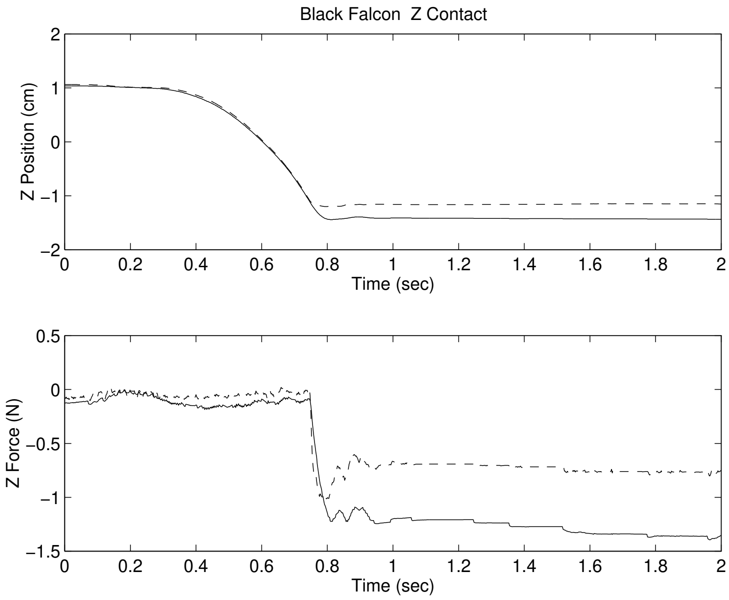

Figure 6-40: Contact response for the Black Falcon slave and Phantom master in the z direction using the Inverse Jacobian controller. The solid line represents the master, and the dashed line represents the slave.

as expected with a 20000 N/m joint 2 gain. The resulting freespace forces are nearly zero. Then, when contact is made, a very sharp increase in force occurs in both the master and the slave which settles to a steady state value of 0.7 N in the slave and 1.4 N in the master as pressure is applied by the user.

A reasonable question to ask is why is this axis better than the others? This is certainly an area for future investigation. We suggest the reason is simply the quality of the macro and micro freedoms involved. The macro freedom, joint 2, has a backlash free transmission, is lightweight, and has excellent encoder resolution because four encoder signals are averaged in determining its position. The micro freedom, joint 4, is low friction because it is actuated by only one motor. This simple combination makes this combination of axes most similar to our original macro-micro testbed studied in Chapter 3. If the design of the other axes could be improved such that they achieved these characteristics, overall system performance might be improved.

6.4.3 Discrimination Tests

As in the Silver Falcon, we found that the lowest level of force which a user could discriminate correlates well with the wrist backdrive friction levels. In these tests, we used the Tool Handle haptic interface as a master manipulator instead of the Phantom (**?**). We also used the Inverse Jacobian controller. We used a 5:1 motion scaling and a 2:1 force scaling, because this is the same setup used during our demonstration of suturing described below. A loop of string was held in the fingertips at one end and attached to a digital force gage (Mark 10 Model BG2) at the other. With my eyes closed, I pulled until I first felt a force. The location of the sensor was moved every time so that I could not learn the position where the force would appear. Five values were taken in each direction and the values averaged. The error represents one standard deviation.

$$f_{dx} = 0.34 \pm 0.08\ N \tag{6.17}$$
$$f_{dy} = 0.58 \pm 0.3\ N \tag{6.18}$$
$$f_{dz} = 0.51 \pm 0.09\ N \tag{6.19}$$

6.5 Features

There are a number of additional features which can be implemented when a teleoeperator is used. Below we discuss motion scaling and indexing.

6.5.1 Motion Scaling

Motion scaling is simple to implement. The slave is commanded to track scaled versions of the master motions. Rotational motions are not scaled. We typically want to allows large master motions to correspond to small slave motions, as this makes the slave more steady, in that jerky master movements are made smaller and less noticable. It also effectively increases the position resolution of the master. We tried values ranging from 1:1 to 5:1. The value to choose is task dependent. 5:1 be good when the surgeon is performing 1/2 in slave motions, but is inconvenient if he is making 2 in slave motions. For suturing, which we discuss below, I found 2:1 motion scaling to work well.

6.5.2 Indexing

Indexing is the concept of detaching the master from the slave (via the controller) in order to reposition the master within its workspace. This is analagous to lifting a computer mouse from its pad (disengaging it from the cursor) and moving it back to the center of the mouse pad. This is again straightforward to implement, and makes sense for positions. It does not make sense to index orientations because if master and slave orientations become misaligned it becomes very difficult for the surgeon to determine how master motions correspond to slave motions. Position indexing is especially helpful when large motion scaling factors are used. We found ourselves indexing frequently when setting up the slave with respect to a given task.

6.6 Tasks

We demonstrated two tasks which show different aspects of the system. The first task was suturing, which is obviously relevent to MIS, and has been described as the most difficult task during surgery aside form knot tying....(**?**). Suturing is primarily a geometric task. That is, success depends on whether the system has sufficient degrees of freedom, workspace, and the appropriate kinematics to make the required motions.

The second test we tried is a tube and wire test, where we push a piece of clear plastic tubing along a wire bent into “S” shaped curves. This task requires similar mobility to suturing, but also requires contact with a much stiffer environment, namely a rigid metal wire. As a result, force reflection becomes much more important because small motions can create large forces which are difficult to detect visually.

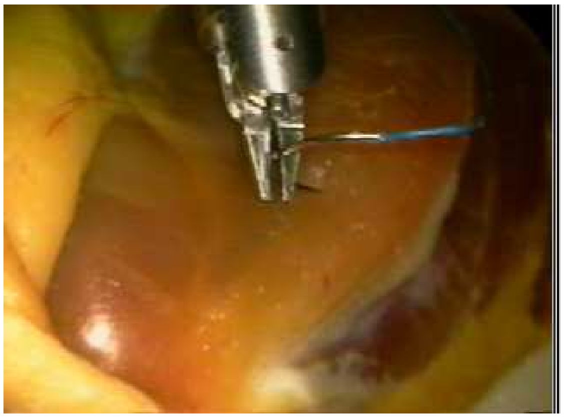

Figure 6-41: Suturing along a line roughly parallel with the instrument shaft. Beginning a stitch.

Figure 6-42: Suturing along a line roughly parallel with the instrument shaft. Rolling about the fingers and pushing the needle through the tissue.

6.6.1 Suturing

Suturing is considered to be one of the more difficult surgical tasks. When asked, surgeons uniformly ask whether or not suturing will be possible using our technology.

To demonstrate our ability to suture along arbitrary suture lines, I made stitches in muscle tissue, specifically a chicken leg with the skin removed. We used an Ethicon Ethibond polyester suture (3-0) with a curved, tapered SH needle. I found I could make a row of stitches along different lines relative to the instrument shaft. For example, I could suture along a line parallel with the instrument shaft, as can be done with difficulty (by some surgeons) using conventional MIS instruments, see Figures 6-41 through 6-44. Also, I could suture along a line perpendicular to the shaft which is essentially impossible using conventional MIS instruments, see Figures 6-45 through 6-48. It seemed clear that the instrument had sufficient degrees of freedom and that the geometry of the wrist allowed this to occur.

We tried suturing both with and without force reflection. Interestingly, we found force reflection to be more of an annoyance than a help.

- Our first comment is that the quality of our system simply is not good enough to help during suturing. Specifically freespace motions still do not yet feel free enough. That is there are background forces which cause fatigue during fine motions required for suturing.
- The second problem is that there is a sufficient deadband in the forces which

Figure 6-43: Suturing along a line roughly parallel with the instrument shaft. Pulling the needle from the tip out of the tissue.

Figure 6-44: Suturing along a line roughly parallel with the instrument shaft. A completed row of stitches.

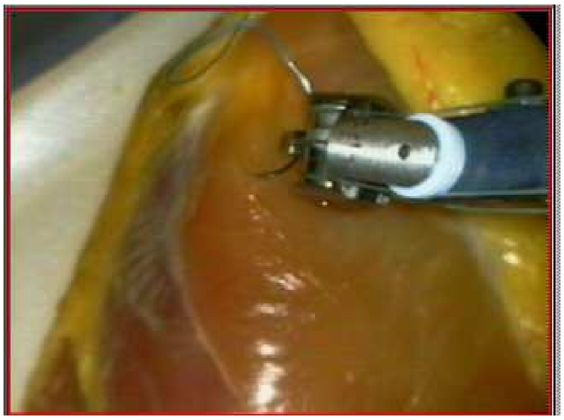

Figure 6-45: Suturing along a line perpendicular with the instrument shaft. Beginning a stitch.

Figure 6-46: Suturing along a line perpendicular with the instrument shaft. Pulling the needle from the tip out of the tissue.